Remote Sensing of Environment 123 (2012) 163–174

Contents lists available at SciVerse ScienceDirect

Remote Sensing of Environment

journal homepage: www.elsevier.com/locate/rse

Water properties in Chesapeake Bay from MODIS-Aqua measurements

SeungHyun Son [a,b], Menghua Wang [a,*]

[a] NOAA National Environmental Satellite, Data, and Information Service, Center for Satellite Applications and Research, E/RA3, Room 102, 5200 Auth Road, Camp Springs, MD 20746, USA
[b] CIRA at Colorado State University, Fort Collins, CO 20523, USA

ARTICLE INFO

Article history:
Received 24 August 2011
Received in revised form 13 January 2012
Accepted 11 March 2012
Available online 19 April 2012

Keywords:
Ocean color remote sensing
Water quality
Chesapeake Bay

ABSTRACT

This study evaluates the performance of ocean color products derived from measurements of the Moderate Resolution Imaging Spectroradiometer (MODIS) on the satellite Aqua using the standard near-infrared (NIR) and the shortwave infrared (SWIR)-based atmospheric correction algorithms in the Chesapeake Bay. The MODIS-Aqua-derived normalized water-leaving radiances, $nL_w(\lambda)$, and chlorophyll-a (Chl-a) data are compared with in situ radiometric measurements from the NASA SeaWiFS Bio-optical Archive and Storage System (SeaBASS) database and Chl-a data from the Chesapeake Bay Water Quality Database. Results show that, using the NIR-SWIR combined ocean color data processing, improved $nL_w(\lambda)$ and Chl-a data products can be produced in the Chesapeake Bay. However, Chl-a data are still overestimated in some Chesapeake Bay regions, in particular, in the upper bay region where waters are strongly influenced by the total suspended sediment (TSS) concentration. Specifically, using the NIR-SWIR approach, mean ratios of MODIS-derived and in situ-measured $nL_w(\lambda)$ at wavelengths of 412, 443, 488, 531, 551, and 667 nm for the Chesapeake Bay are 1.288, 1.093, 0.998, 0.946, 0.908, and 0.865, respectively, while mean Chl-a values over the region from satellite-derived and in situ-measure data are 11.14 and 10.28 $mg \cdot m^{-3}$, respectively. Based on a strong correlation relationship between TSS and water diffuse attenuation coefficient, a regional TSS algorithm for the Chesapeake Bay has been developed and validated, with mean ratio of 1.064 between MODIS-derived and in situ-measured TSS data. Therefore, using the NIR-SWIR algorithm for MODIS-Aqua ocean color data processing, $nL_w(\lambda)$, Chl-a, and TSS data from 2002 to 2010 for the Chesapeake Bay have been generated and used for characterizing the water properties in the region, showing strong seasonal and interannual variability, as well as important spatial variations in the region.

Published by Elsevier Inc.

1. Introduction

The Chesapeake Bay has highly productive waters along the U.S. East Coast region with about 2.3×10^3 $m^3 \cdot s^{-1}$ of river freshwaters on average flow into the Chesapeake Bay, including dissolved and particulate materials (Schubel & Pritchard, 1986). Bio-optical properties of the Chesapeake Bay waters are strongly influenced by complex constituents of high phytoplankton concentration, dissolved organic matter (DOM), and total suspended sediment (TSS) (Gallegos et al., 1990; Gitelson et al., 2007; Harding et al., 2005; Tzortziou et al., 2007). Thus, satellite-derived chlorophyll-a (Chl-a) concentrations using bio-optical models for open ocean (Case-1) waters (O'Reilly et al., 1998) are often overestimated in the turbid coastal waters (Magnuson et al., 2004; Werdell et al., 2009). There have been considerable efforts in developing bio-optical models for Chl-a products from satellite ocean color sensors such as the Sea-Viewing Wide Field-of-view Sensor (SeaWiFS) and the Moderate Resolution Imaging Spectroradiometer (MODIS) on the Aqua in the Chesapeake Bay waters (Gitelson et al., 2007; Magnuson et al., 2004; Tzortziou et al., 2007; Werdell et al., 2009). Other water optical properties, such as apparent and inherent optical properties, in the region have also been studied to develop bio-optical models for the ocean color products in the Chesapeake Bay (Gallegos & Neale, 2002; Tzortziou et al., 2006, 2007; Zawada et al., 2007). However, an appropriate bio-optical algorithm for the Chesapeake Bay region is still an outstanding issue for satellite ocean color remote sensing.

In addition to uncertainties in bio-optical algorithms for the region, there are also issues with effective atmospheric correction algorithms for deriving accurate satellite ocean color products in turbid coastal waters, particularly for the black pixel assumption in the near-infrared (NIR) bands that are used for atmospheric correction (Shi & Wang, 2009c; Wang, 2007; Wang & Shi, 2005). For open oceans, two MODIS-measured NIR radiances at bands of 748 and 869 nm are used for atmospheric correction (Gordon, 1997; Gordon & Wang, 1994; IOCCG, 2010), which is in the NASA standard routine data processing for deriving ocean color products. However, the NIR black ocean assumption is invalid for productive and turbid coastal waters, and significant efforts have been made to estimate the NIR ocean contributions in order to improve atmospheric correction (Bailey et al., 2010; Ruddick et al., 2000; Siegel et al., 2000; Stumpf et al., 2003; Wang & Shi, 2005). A new approach for atmospheric correction using the shortwave infrared (SWIR) bands at 1240 and

* Corresponding author.
E-mail address: Menghua.Wang@noaa.gov (M. Wang).

0034-4257/$ – see front matter. Published by Elsevier Inc.
doi:10.1016/j.rse.2012.03.009

2130 nm has been developed to derive satellite ocean color products in turbid coastal waters (Wang, 2007). However, due to significant noise issue in the MODIS SWIR bands (Wang & Shi, 2012; Wang et al., 2009b; Werdell et al., 2010), a NIR-SWIR combined atmospheric correction approach for the MODIS-Aqua ocean color data processing has been proposed (Wang & Shi, 2007), i.e., applying the NIR atmospheric correction algorithm for the non-turbid ocean while using the SWIR algorithm for turbid waters. In fact, for extremely turbid waters, even the SWIR 1240 nm is not always black (Shi & Wang, 2009c), and the water-leaving radiance contribution at the SWIR 1240 nm needs to be accurately accounted for in the satellite data processing (Wang et al., 2011). It has been shown that improved satellite ocean (water) color products over turbid coastal and inland waters can be produced using the SWIR-based atmospheric correction algorithm (Wang et al., 2007, 2009b, 2011), and these data have been used for various studies and applications in coastal ocean regions (Nezlin et al., 2008; Shi & Wang, 2007, 2008, 2009a, 2009b, 2010; Shi et al., 2011; Son et al., 2011).

In this study, we evaluate and analyze the performance of the MODIS-Aqua-derived ocean color products, including normalized water-leaving radiances ($nL_w(\lambda)$) and Chl-a data, from the standard NIR and the NIR-SWIR combined atmospheric correction methods in the Chesapeake Bay. The satellite-derived product uncertainties in the Chesapeake Bay are investigated using in situ measurements. Furthermore, a regional total suspended sediment (TSS) algorithm for the Chesapeake Bay has been developed and applied to MODIS-Aqua data. Thus, using the NIR-SWIR-based satellite ocean color data processing, MODIS-Aqua-measured $nL_w(\lambda)$, Chl-a, and TSS data from 2002 to 2010 are generated and used to characterize water properties in the Chesapeake Bay.

2. Data and methods

In this section, both in situ and satellite data used for study of the Chesapeake Bay are described and discussed. In particular, following Magnuson et al. (2004), three different regions in the Chesapeake Bay are defined (Fig. 1): Lower Bay (region south of 37.6°N), Middle Bay (region in 37.6–38.6°N), and Upper Bay (region north of 38.6°N).

2.1. In situ data

In situ Chl-a data from 2002 to 2008 were obtained from a long-term Water Quality Database for the Chesapeake Bay, which has been maintained by the Chesapeake Bay Program (www.chesapeakebay.net/wquality.htm) (Fig. 1), to evaluate MODIS-Aqua-derived Chl-a data using NIR and NIR-SWIR atmospheric correction methods and a standard bio-optical algorithm (O'Reilly et al., 1998, 2000). Since there are up to three coincident in situ measurements at each station, average values were calculated from multiple measurements.

In situ radiometric data from 2002 to 2010 were also obtained from the NASA SeaWiFS Bio-optical Archive and Storage System (SeaBASS) database (Werdell & Bailey, 2005) for the Chesapeake Bay and adjacent waters (http://seabass.gsfc.nasa.gov/) to evaluate MODIS-Aqua ocean color products in the region (Fig. 1). Normalized water-leaving radiance spectra ($nL_w(\lambda)$) (Gordon, 2005; Gordon & Wang, 1994; Morel & Gentili, 1996; Wang, 2006) are derived from MODIS-Aqua measurements over the region. Since the wavelengths at which the radiance data were measured from the SeaBASS are not exactly matched with those from the satellite measurements, we simply used the nearest wavelength values of in situ $nL_w(\lambda)$ at wavelengths of 411, 443, 489, 510, 530, 550, and 670 nm.

In addition, in situ TSS data and the water diffuse attenuation coefficient for the downwelling photosynthetically available radiation (PAR) (K_d(PAR)) measurements from 1984 to 2010 in the Chesapeake Bay were obtained from the Chesapeake Bay Program for developing a regional TSS algorithm for satellite data applications. The in situ TSS data in the Chesapeake Bay have also been used for the regional satellite TSS algorithm validation, as well as TSS product evaluations.

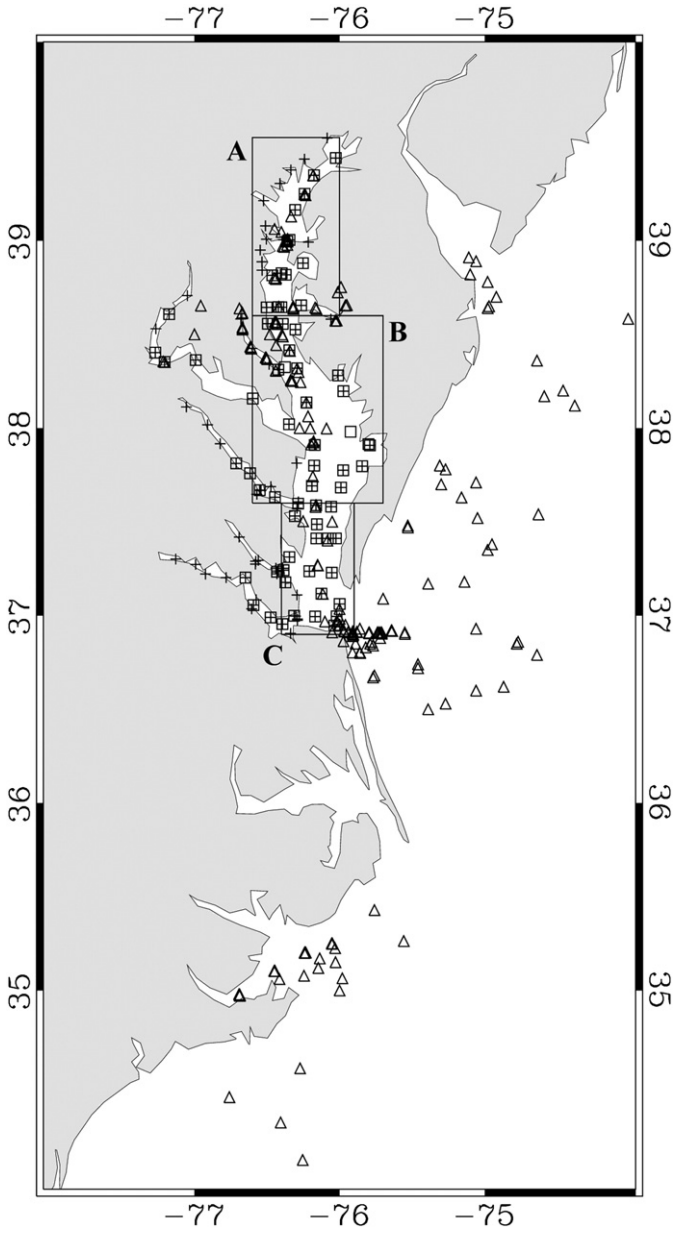

Fig. 1. Map of the Chesapeake Bay and adjacent area with in situ observation locations. Squares and crosses indicate locations of Chl-a and TSS measurements from the Chesapeake Bay Water Quality Database, respectively, and triangles indicate locations of radiometric measurements from the NASA SeaBASS database. The three boxes (A, B, and C) are for Upper, Middle, and Lower Bays, respectively.

2.2. Satellite ocean color data

The NASA Ocean Biology Process Group (OBPG) has recently reprocessed all satellite ocean color products (R2009), including MODIS-Aqua data, with some important changes and updates in sensor-specific calibration, ancillary data sources, product format, and some algorithms, e.g., (Ahmad et al., 2010; Bailey et al., 2010). Both the previous version (Ver5.2) and the current processed (R2009) daily MODIS-Aqua Level-2 ocean color products, derived using the standard-NIR atmospheric correction algorithm with the NIR radiance corrections (Bailey et al., 2010; Stumpf et al., 2003), were obtained from the NASA ocean color website

(http://oceancolor.gsfc.nasa.gov) for the period of July 2002 to December 2008. In addition, MODIS Level-2 ocean color products were generated using the NIR-SWIR combined atmospheric correction algorithm (Wang, 2007; Wang & Shi, 2007; Wang et al., 2009b) with MODIS-Aqua Level-1B data from the NASA MODIS Adaptive Processing System (MODAPS) Services website for the period of July 2002 to December 2010. Those Level-2 data were remapped to a standard projection at 1-km spatial resolution and then processed to generate various product composite images.

Pixels from a 5×5 box centered at a location of in situ measurements were extracted from MODIS Level-2 data processed with the NIR (both in Ver5.2 and R2009 versions) and the NIR-SWIR atmospheric correction algorithms and compared to in situ measurements. For the data match-up analyses (satellite vs. in situ), we have followed the procedure of Wang et al. (2009b). In addition, time series of monthly composite images from MODIS-Aqua NIR- and NIR-SWIR-derived ocean color data from July 2002 to December 2010 were produced for the three Chesapeake Bay regions defined in Fig. 1. Regional averages of ocean color parameters are calculated for the seasonal and interannual time series.

3. Product evaluations and development

3.1. Comparison of satellite-derived and in situ-measured $nL_w(\lambda)$

Fig. 2 provides comparisons of MODIS-Aqua-derived $nL_w(\lambda)$ products at wavelengths of 412, 443, 488, 531, 551, and 667 nm using the NIR-SWIR combined atmospheric correction algorithm (Wang & Shi, 2007; Wang et al., 2009b) with in situ-measured $nL_w(\lambda)$ data from the SeaBASS database in the Chesapeake Bay and adjacent areas. In general, the MODIS-Aqua NIR-SWIR-derived $nL_w(\lambda)$ data are well correlated to those from in situ measurements for most wavelengths. Specifically, while the MODIS-derived $nL_w(\lambda)$ data at 488, 531, and

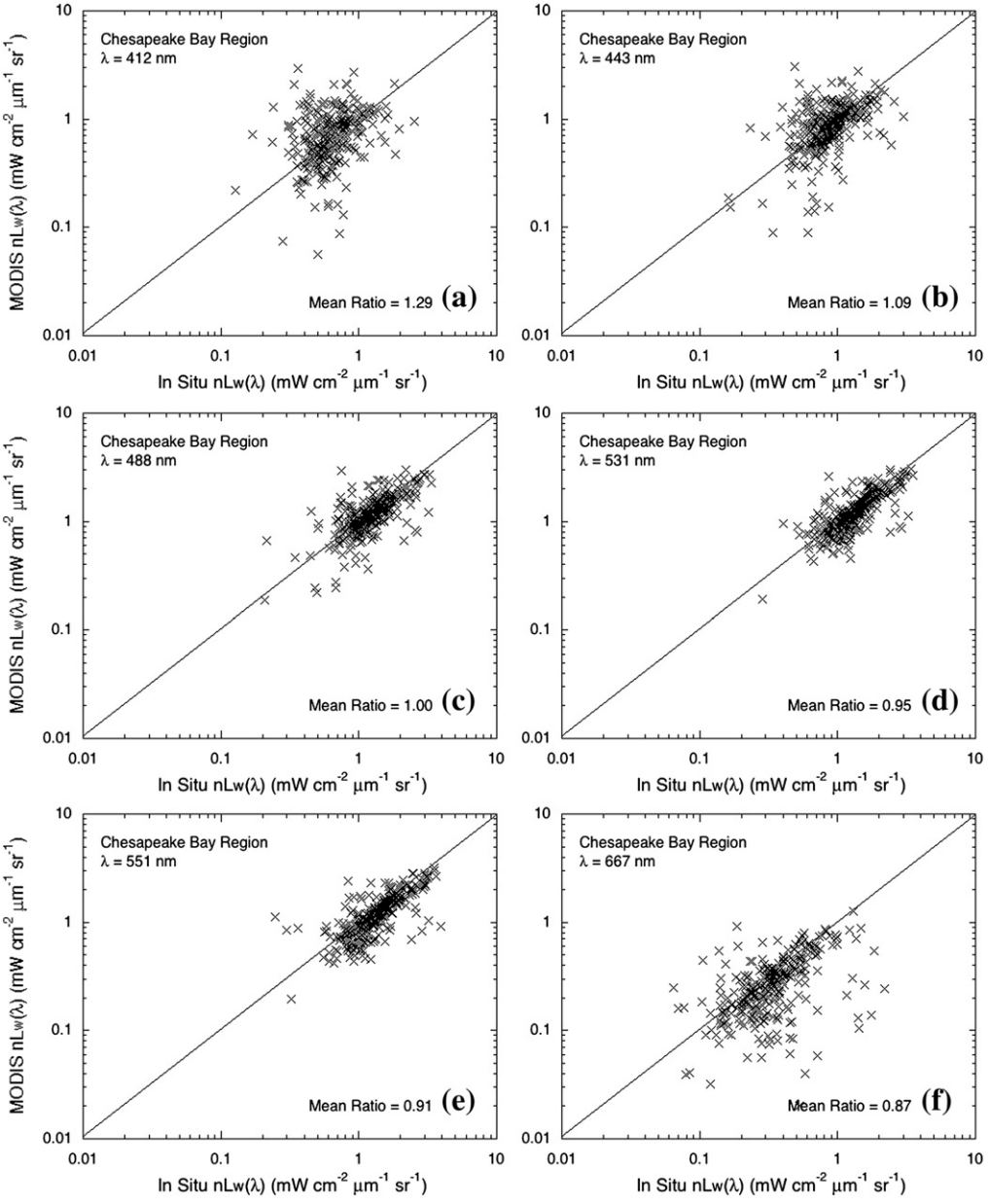

Fig. 2. Match-up comparisons of the MODIS-derived $nL_w(\lambda)$ with the SeaBASS in situ $nL_w(\lambda)$ measurements at wavelengths (a) 412, (b) 443, (c) 488, (d) 531, (e) 551, and (f) 667 nm using the NIR-SWIR combined atmospheric correction algorithm.

Table 1
Statistics of match-up comparisons between the MODIS-derived and in situ-measured $nL_w(\lambda)$ in the mid-eastern US coastal waters.

Data	Parameter	$nL_w(412)$	$nL_w(443)$	$nL_w(488)$	$nL_w(531)$	$nL_w(551)$, $nL_w(547)$	$nL_w(667)$
In-situ	Mean[a]	0.681	0.929	1.310	1.433	1.451	0.400
	STD[a]	0.300	0.395	0.533	0.589	0.634	0.291
NIR R2009	Mean[a]	0.497	0.671	0.909	1.022	1.007	0.208
	STD[a]	0.249	0.291	0.387	0.438	0.457	0.149
	Mean ratio	0.775	0.755	0.710	0.729	0.719	0.570
	Ratio STD	0.369	0.263	0.173	0.170	0.259	0.283
NIR-SWIR	Mean[a]	0.788	0.940	1.243	1.308	1.259	0.298
	STD[a]	0.425	0.434	0.501	0.543	0.560	0.196
	Mean ratio	1.288	1.093	0.998	0.946	0.908	0.865
	Ratio STD	0.896	0.605	0.380	0.294	0.365	0.573
Data #		281	294	306	306	306	302

[a] Unit of $mW \cdot cm^{-2} \cdot \mu m^{-1} \cdot sr^{-1}$.

551 nm are well correlated to the in situ $nL_w(\lambda)$ measurements, the matchup comparison between MODIS-Aqua and the in situ $nL_w(\lambda)$ measurements at wavelengths of 412 and 667 nm is a little noisy. However, the MODIS NIR-SWIR-derived $nL_w(\lambda)$ data are improved compared with the MODIS NIR-derived $nL_w(\lambda)$ data. Results from statistical analyses are shown in Table 1.

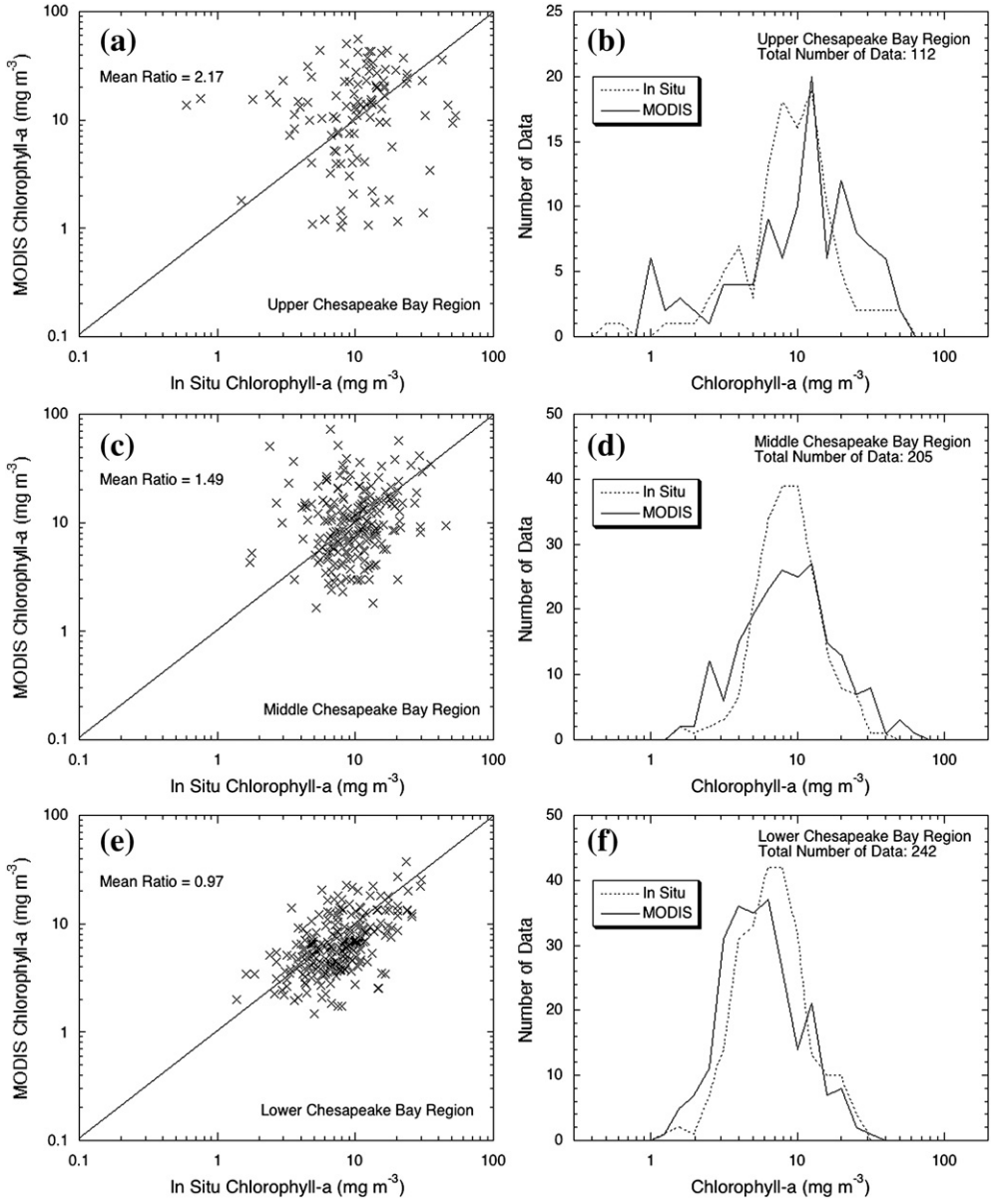

Fig. 3. Comparison of match-up and histogram results between the MODIS-derived Chl-a using the NIR-SWIR combined method and the in situ Chl-a measurements from the Chesapeake Bay Water Quality Database for the Chesapeake Bay sub-regions of (a) and (b) Upper Bay, (c) and (d) Middle Bay, and (e) and (f) Lower Bay.

The MODIS NIR R2009 $nL_w(\lambda)$ data are generally underestimated for most wavelengths, compared with in situ $nL_w(\lambda)$ measurements. Mean values of the MODIS-Aqua NIR R2009 $nL_w(\lambda)$ at wavelengths of 412, 443, 488, 531, 547 (551), and 667 nm are 0.50, 0.67, 0.91, 1.02, 1.01, and 0.21 $mW \cdot cm^{-2} \cdot \mu m^{-1} \cdot sr^{-1}$, respectively, compared to the corresponding in situ mean values of 0.68, 0.93, 1.31, 1.43, 1.45, and 0.40 $mW \cdot cm^{-2} \cdot \mu m^{-1} \cdot sr^{-1}$, respectively. Mean values of MODIS-Aqua NIR-SWIR-derived $nL_w(\lambda)$ data are relatively closer to those from the in situ measurements in most of the wavelengths, with the corresponding mean values of 0.79, 0.94, 1.24, 1.31, 1.26, and 0.30 $mW \cdot cm^{-2} \cdot \mu m^{-1} \cdot sr^{-1}$, respectively. However, some slight overestimations for NIR-SWIR-derived $nL_w(\lambda)$ at 412 and 443 nm are observed. Results with a mean ratio of MODIS to in situ $nL_w(\lambda)$ measurements show improvements in the MODIS NIR-SWIR-derived $nL_w(\lambda)$ data (mean ratios of 0.87–1.29, depending on the wavelength), compared with the MODIS NIR-derived $nL_w(\lambda)$ data (mean ratios of 0.57–0.75). However, as expected, the standard deviation (STD) values are higher in MODIS-Aqua NIR-SWIR measurements due to sensor noise in the MODIS-Aqua SWIR bands (Wang, 2007; Wang & Shi, 2012; Werdell et al., 2010).

3.2. Comparison of satellite-derived and in situ-measured Chl-a data

In situ Chl-a measurements collected from the Chesapeake Bay Program Office from July 2002 to December 2008 are used for comparison with MODIS-Aqua-derived Chl-a data using the NIR-SWIR method for three different regions in the Chesapeake Bay (Fig. 3). The MODIS NIR-SWIR-derived Chl-a data are overestimated in Upper and Middle Bays (Fig. 3a and c), although the MODIS-Aqua-derived Chl-a data in Middle Bay are relatively better than those in Upper Bay. In Lower Bay, the MODIS-Aqua-derived Chl-a data are well correlated to those from the in situ measurements (Fig. 3e). Statistics values in match-up comparisons between the MODIS-derived Chl-a using the NIR (Ver5.2 and R2009) and the NIR-SWIR methods and in situ Chl-a measurements are provided in Table 2. The mean ratio results in Upper Bay show that the MODIS-Aqua-derived Chl-a data are significantly overestimated compared with in situ Chl-a data. However, mean ratio values (MODIS to in situ) are better for the MODIS Chl-a using the NIR-R2009 (2.37) and NIR-SWIR (2.17) methods than those with the NIR-Ver5.2 Chl-a (3.37). In Middle Bay, all MODIS-derived Chl-a data are also overestimated, but mean ratios (MODIS to in situ) are reduced compared with those in Upper Bay. Similar to results in Upper Bay, mean ratios are relatively better for the MODIS NIR-R2009 (1.75) and NIR-SWIR (1.49) in Chl-a data than those from the MODIS NIR-Ver5.2 Chl-a (2.46). In Lower Bay, MODIS-Aqua-derived Chl-a data using NIR-Ver5.2 and NIR-R2009 methods are overestimated with mean ratio values of 1.73 and 1.58, respectively, while Chl-a data from the NIR-SWIR are significantly improved with a mean ratio of 0.97.

Histogram results of MODIS Chl-a data derived using the NIR-SWIR method are compared with those of in situ data for the three subregions in the Chesapeake Bay (Fig. 3b, d, and f). MODIS NIR-SWIR-derived Chl-a data are biased high in Upper Bay (Fig. 3b). Mean values of the in situ- and MODIS NIR-SWIR-derived Chl-a data are 12.32 and 16.03 $mg \cdot m^{-3}$, respectively. However, the MODIS NIR-SWIR Chl-a concentrations are relatively lower than those of the MODIS Chl-a using the NIR-Ver5.2 (25.90 $mg \cdot m^{-3}$) and the NIR-R2009 (18.83 $mg \cdot m^{-3}$). Note that results with the MODIS Chl-a data using the NIR atmospheric correction algorithm are not shown in Fig. 3, but results in statistics are provided

Table 2
Statistics of match-up comparisons between the MODIS-derived and in situ-measured chlorophyll-a in the main stem of the Chesapeake Bay.

Area	Type	Mean[a]	STD[a]	Median[a]	Mean ratio	Data #
CB all	In situ	10.28	6.70	8.68	–	559
	NIR (Ver5.2)	19.29	14.08	16.10	2.33	
	NIR (R2009)	14.86	11.01	12.50	1.80	
	NIR-SWIR	11.14	9.65	8.10	1.40	
Upper Bay	In situ	12.32	9.47	10.17	–	112
	NIR (Ver5.2)	25.90	15.83	23.54	3.37	
	NIR (R2009)	18.83	14.92	14.77	2.37	
	NIR-SWIR	16.03	12.44	13.59	2.17	
Middle Bay	In Situ	10.99	6.14	9.87	–	205
	NIR (Ver5.2)	22.38	14.89	19.28	2.46	
	NIR (R2009)	15.80	9.20	14.28	1.75	
	NIR-SWIR	12.64	10.43	9.72	1.49	
Lower Bay	In situ	8.73	5.10	7.63	–	242
	NIR (Ver5.2)	13.62	9.77	11.29	1.73	
	NIR (R2009)	12.22	9.56	10.20	1.58	
	NIR-SWIR	7.61	5.19	6.06	0.97	

[a] Unit of $mg \cdot m^{-3}$

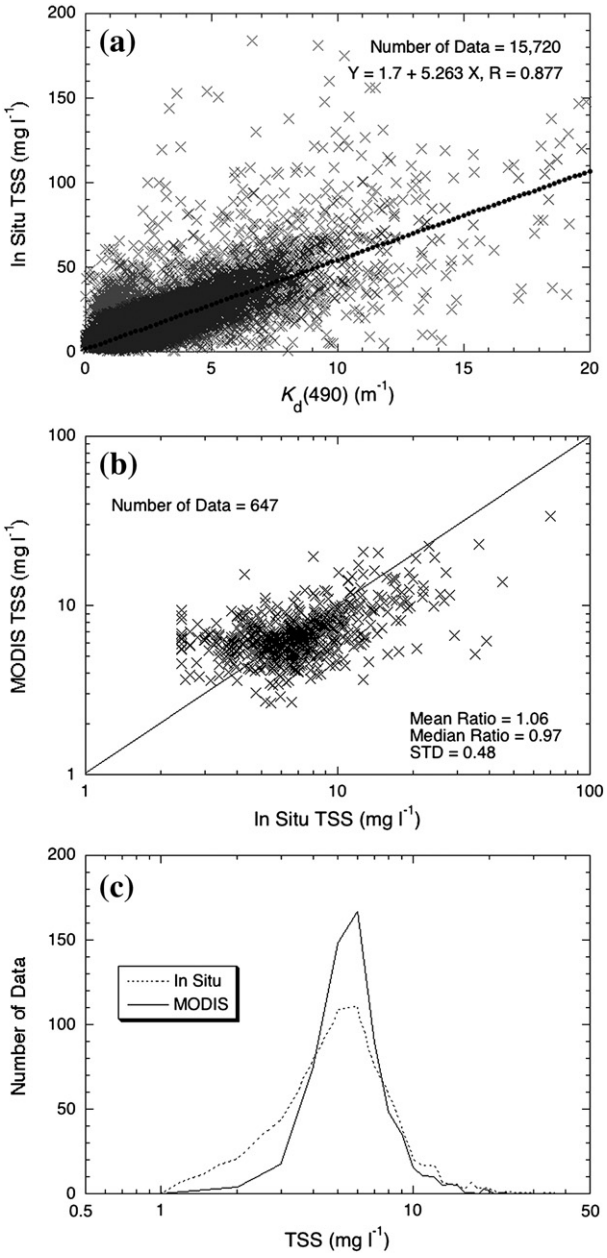

Fig. 4. (a) Comparison between the in situ $K_d(490)$ and TSS measurements obtained from the Chesapeake Bay Water Quality Database for the Chesapeake Bay (black dotted line indicates a best fit), (b) match-up comparison of the in situ TSS measurements with the MODIS-derived TSS using the NIR-SWIR combined method, and (c) histogram results for the in situ (dashed line) and the MODIS-NIR-SWIR-derived (solid lines) TSS measurements.

in Table 2. In Middle Bay, the distribution shape of MODIS NIR-SWIR-derived Chl-a data with a mean of 12.64 mg·m^{-3} is similar to that of in situ measurements, which have a mean of 10.99 mg·m^{-3} (Fig. 3d). The MODIS NIR-derived Chl-a data are distributed with a positive bias, and mean values are considerably higher (22.38 and 15.80 mg·m^{-3} for NIR-Ver5.2 and NIR-R2009, respectively) than those of the in situ Chl-a data. The histogram comparison for Lower Bay shows that the distribution shape of the MODIS NIR-SWIR-derived Chl-a is similar to that of the in situ measurements, and the mean value (7.61 mg·m^{-3}) is slightly lower than that of the in situ Chl-a (8.73 mg·m^{-3}) (Fig. 3f). In comparison, the MODIS NIR-Ver5.2 and NIR-R2009-derived Chl-a data are biased high with mean values of 13.62 and 12.22 mg·m^{-3}, respectively.

3.3. Total suspended sediment (TSS) model for the Chesapeake Bay

In situ TSS and K_d(PAR) (water diffuse attenuation coefficient for the downwelling photosynthetically available radiation) measurements with more than ~15,700 data were obtained in the main stem of the Chesapeake Bay from 1984 to 2010. The K_d(PAR) data were converted to the diffuse attenuation coefficient at the wavelength of 490 nm, K_d(490), using a relationship for the Chesapeake Bay, which was derived in Wang et al. (2009a). In situ TSS data were then compared to in situ K_d(490) data to derive a regional TSS algorithm for satellite applications (Fig. 4a). The comparison results show that TSS data are strongly correlated to the K_d(490) in the Chesapeake Bay with a correlation coefficient of 0.877, i.e., TSS can be linearly related to K_d(490) in the Chesapeake Bay as

$$TSS = 1.7 + 5.263\,K_d(490)\ \text{mg l}^{-1}, \quad (1)$$

where K_d(490) is in m^{-1}. The linear relationship (Eq. 1) is applied to the MODIS-Aqua K_d(490) data derived using a recently-developed semi-analytical K_d(490) model for turbid coastal waters (Wang et al., 2009a). MODIS-Aqua-derived TSS data from Eq. (1) can then be compared with in situ TSS measurements for evaluation and validation. For the matchup comparison, MODIS-Aqua-derived TSS data were extracted from a 5×5 box centered at a location of the in situ measurements as the same procedure for Chl-a and $nL_w(\lambda)$ matchup comparisons (Wang et al., 2009b). Fig. 4b provides these comparison results, showing that MODIS-Aqua-derived TSS data using the new regional algorithm are reasonably accurate. The mean ratio of the MODIS-Aqua-derived TSS to the in situ-measured TSS is 1.064 with the STD of 0.478. Furthermore, Fig. 4c compares histogram results of MODIS-Aqua-derived TSS data to in situ measurements. Distribution of the MODIS-derived TSS appears well matched with in situ TSS data, although less MODIS-measured TSS data are distributed in the low values (Fig. 4c). Both MODIS and in situ TSS values range from ~1.0 mg·l^{-1} to ~20 mg·l^{-1}, and both peaks are located at ~5–6 mg·l^{-1} as shown in Fig. 4c. Thus, MODIS-Aqua-derived TSS data can be used to study and characterize water properties in the Chesapeake Bay.

4. Characterization of water properties for the Chesapeake Bay

4.1. Satellite $nL_w(\lambda)$ composite images

Seasonal climatology images (July 2002 to December 2010) of the MODIS-Aqua-derived $nL_w(\lambda)$ at 443, 555, 645, and 859 nm using the NIR-SWIR method are shown in Fig. 5. Fig. 5a–d, e–h, i–l, and m–p are results for $nL_w(\lambda)$ at 443, 555, 645, and 859 nm (spring, summer, fall, and winter) in the Chesapeake Bay, respectively. General spatial distributions from MODIS-Aqua seasonal climatology $nL_w(\lambda)$ images are similar in most wavelengths, showing high values in Upper Bay, the eastern area of the Chesapeake Bay, and the northern area of the Chesapeake Bay's mouth (along the peninsula), while lower values are in the western area of Middle Bay. MODIS-Aqua-derived

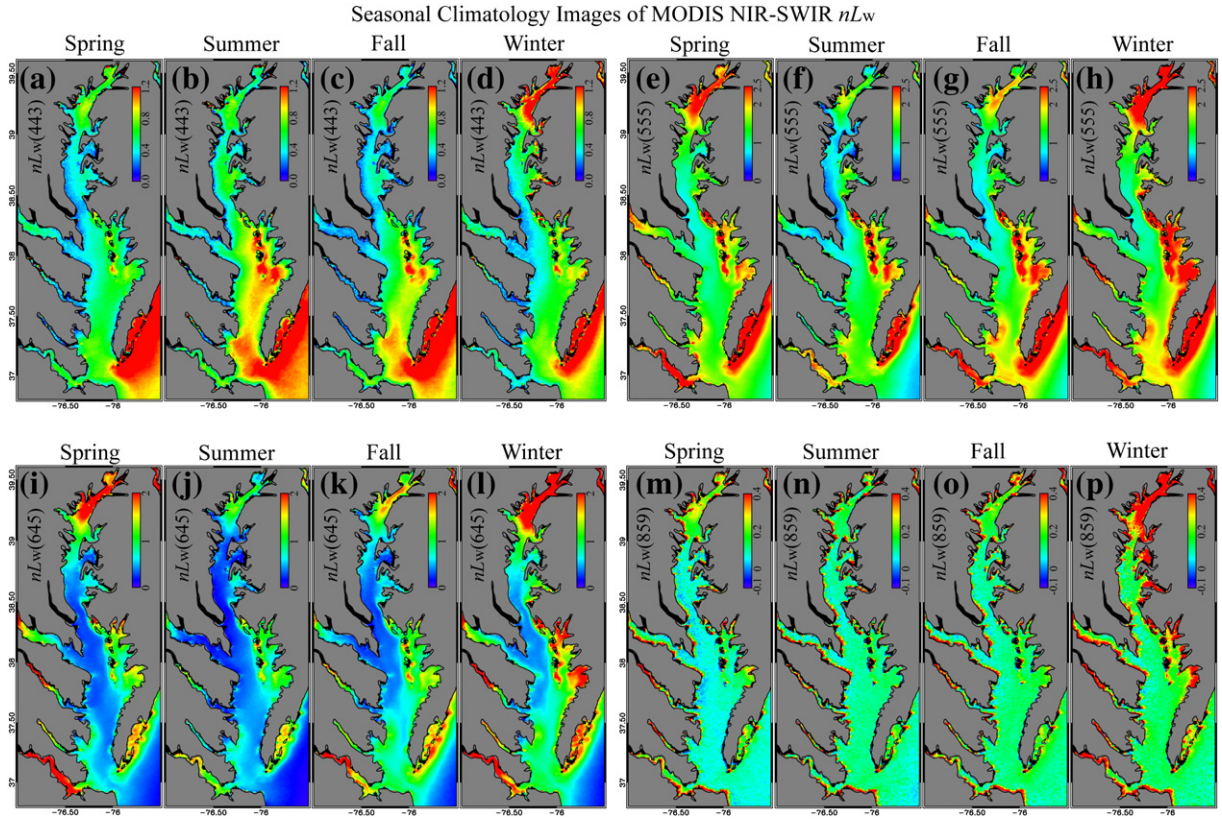

Fig. 5. Seasonal climatology images of the MODIS-derived (a–d) $nL_w(443)$, (e–h) $nL_w(555)$, (i–l) $nL_w(645)$, and (m–p) $nL_w(859)$ for the period of July 2002 to December 2010 using the NIR-SWIR method. Color scales for $nL_w(443)$, $nL_w(555)$, $nL_w(645)$, and $nL_w(859)$ are 0–1.2, 0–2.5, 0–2.0, and −0.1–0.4 mW·cm^{-2}·μm^{-1}·sr^{-1}, respectively.

$nL_w(443)$ values are relatively high offshore from the Chesapeake Bay's mouth (Fig. 5a–d), while high $nL_w(\lambda)$ values at 555, 645, and 859 nm are shown in the Upper Bay region due to significant amount of TSS concentration in the water column. Seasonal peak values appear in winter for all $nL_w(\lambda)$ images and relatively lower values are present in summer to fall for most of the Chesapeake Bay regions. For the Upper Bay region, however, quite high $nL_w(\lambda)$ values at 555, 645, and 859 nm are shown in the spring season.

4.2. Time series of the MODIS $nL_w(\lambda)$ measurements

Time series of monthly averages of MODIS-Aqua-derived $nL_w(443)$, $nL_w(555)$, $nL_w(645)$, and $nL_w(859)$ data in the Upper, Middle, and Lower Bays are obtained from July 2002 to December 2010 (Fig. 6). It is noted that all valid pixels over waters in Boxes A, B, and C (Fig. 1) for the Upper, Middle, and Lower Bays are averaged (spatially and temporally) to produce the corresponding monthly mean value for the region. The temporal patterns are similar for $nL_w(\lambda)$ data at various spectral bands over all locations. However, the seasonal patterns of $nL_w(\lambda)$ are similar in Middle and Lower Bays and somewhat different in Upper Bay depending on years. In particular, $nL_w(555)$ in Lower and Middle Bays is out-of-phase with that in Upper Bay during some years, e.g., in the winter of 2003–2004 and January of 2010. High $nL_w(\lambda)$ values appear generally in winter, and low values are in the summer to fall seasons. In addition, there is a strong interannual variability in MODIS-derived $nL_w(\lambda)$ over all areas. Significantly high $nL_w(\lambda)$ values over all MODIS spectral bands are present in winter 2004, 2005, and 2010 and for $nL_w(859)$ in January of 2003 in Upper Bay. High values of $nL_w(555)$ are apparent in January of 2008 and 2009 in Lower Bay. Relatively lower values of $nL_w(555)$ and $nL_w(645)$ appear in the summer of 2003 over the entire bay. Seasonal variability of $nL_w(443)$ and $nL_w(859)$ is relatively weak and the magnitudes are lower in all regions in 2008 and 2009.

4.3. Satellite Chl-a composite images

Fig. 7 provides seasonal climatology images (July 2002 to December 2010) of the MODIS-Aqua-derived Chl-a data using the NIR-SWIR

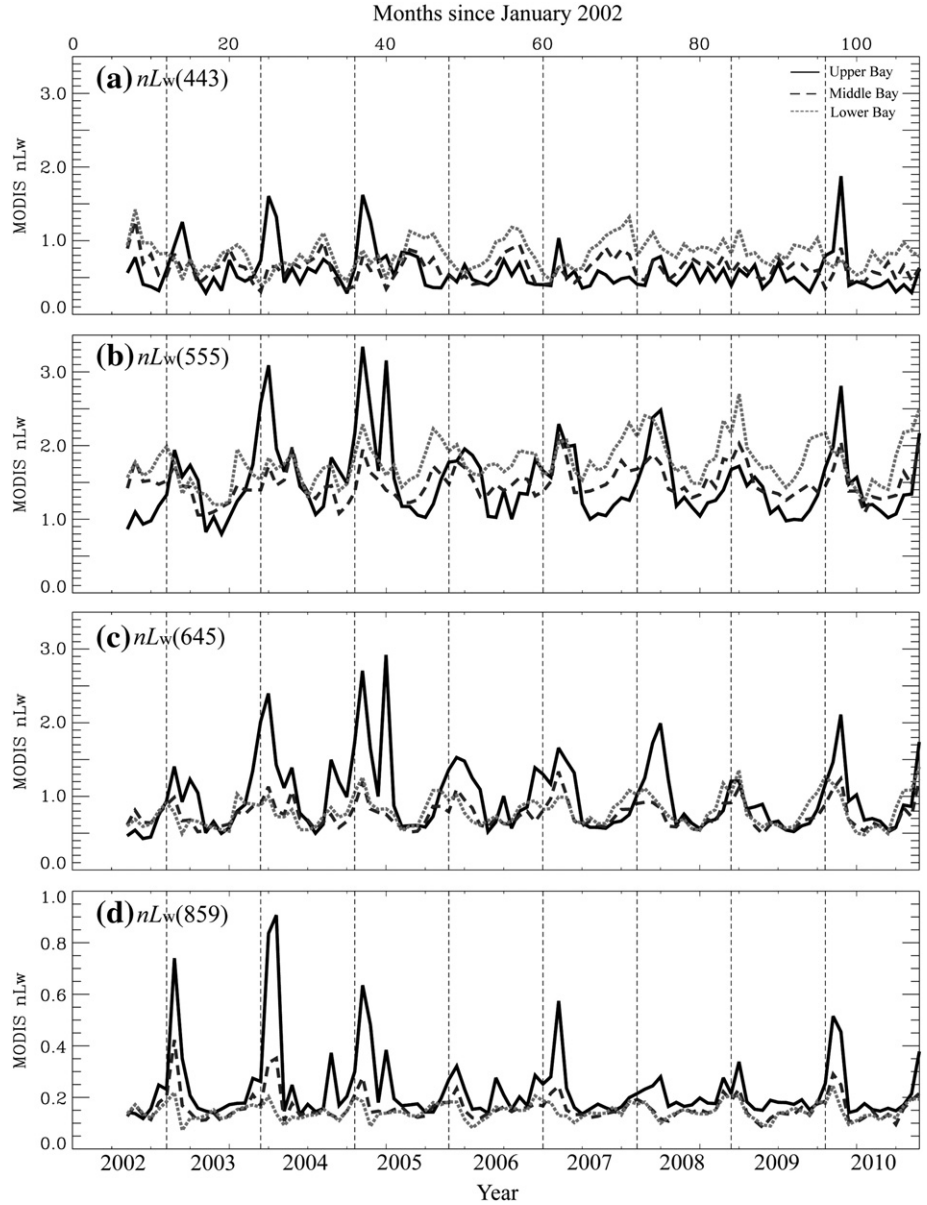

Fig. 6. Time series of the MODIS-derived monthly composites of (a) $nL_w(443)$, (b) $nL_w(555)$, (c) $nL_w(645)$, and (d) $nL_w(859)$ using NIR-SWIR combined method for Upper (solid lines), Middle (dashed lines), and Lower (gray dotted lines) Bays from January 2002 to December 2010.

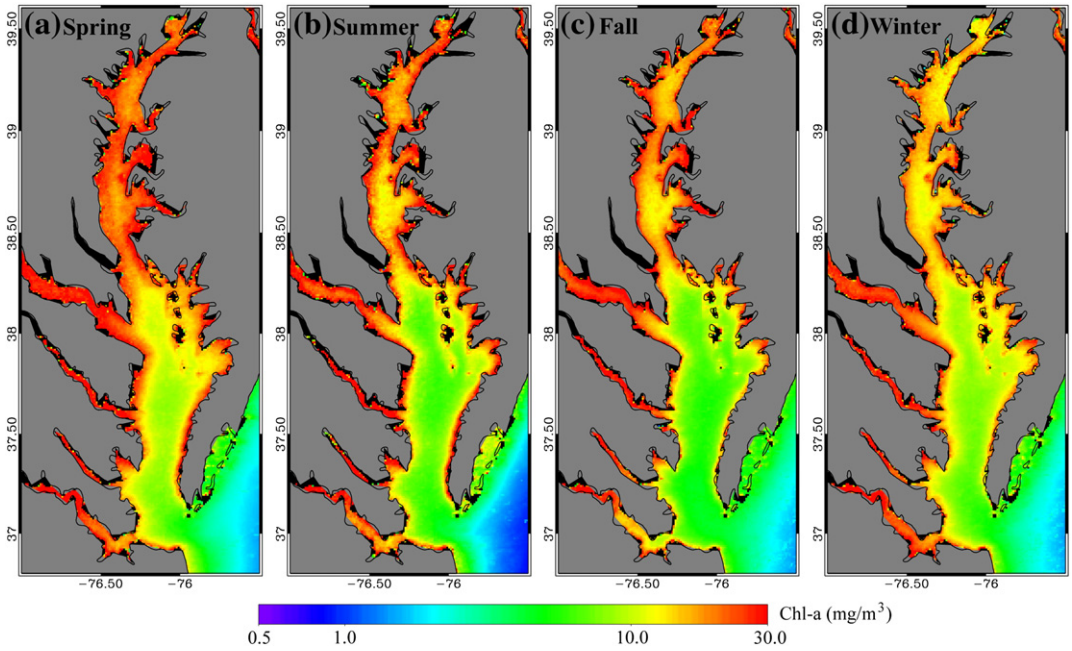

Fig. 7. Seasonal climatology images of the MODIS-Aqua-derived Chl-a for the period of July 2002 to December 2010 using the NIR-SWIR method in the main stem of the Chesapeake Bay in (a) spring (March–May), (b) summer (June–August), (c) fall (September–November), and (d) winter (December–February).

method and the standard OC3 Chl-a algorithm (O'Reilly et al., 1998, 2000) for the main stem of the Chesapeake Bay. Fig. 7a–d are climatology Chl-a images in the Chesapeake Bay for spring, summer, fall, and winter, respectively. In general, spatial distributions of the MODIS seasonal climatology Chl-a images are similar to those of the MODIS $nL_w(\lambda)$ images, showing high Chl-a concentrations located in Upper Bay, river branches, and along the coastal lines, while the lower concentrations are in the central part of Middle to Lower Bays and outside of the Chesapeake Bay. Overall, peak Chl-a values are shown in the spring and the lowest Chl-a concentrations are in the fall in regions of Upper-Middle Bays and winter in Middle-Lower Bays. As discussed previously, Chl-a values are usually overestimated in the Upper and Middle Bay regions, and here we focus on Ch-a variations in the region.

4.4. Time series of Chl-a measurements

Time series of monthly averages of the MODIS-Aqua-derived Chl-a data are constructed for the three regions (Upper, Middle, and Lower Bays) of the Chesapeake Bay (Fig. 8). There is a strong seasonal variability in the Chl-a over the entire bay region. In general, peaks of Chl-a appear in spring (April or May) and the lowest Chl-a concentrations are in winter. Spatially, the highest Chl-a concentrations are in Upper Bay and the lowest Chl-a values in Lower Bay. Although MODIS-Aqua-derived Chl-a concentrations are overestimated in Upper and Middle Bays, the MODIS-derived Chl-a concentrations are relatively reliable for seasonal variations (Fig. 3 and Table 2). Furthermore, results also show a strong interannual variability in Chl-a for the Chesapeake Bay. The interannual variability of Chl-a is somewhat different from that of $nL_w(\lambda)$ images. Anomalously high Chl-a concentrations are apparent in December of 2003, April of 2005, and January of 2010 in both Middle and Lower Bays, while high Chl-a concentrations in summer appeared in 2009 and 2010 in Upper Bay.

4.5. Satellite images and time series of MODIS TSS measurements

Fig. 9 provides seasonal climatology images (July 2002 to December 2010) of MODIS-Aqua-derived TSS data using the NIR-SWIR method and a regional TSS algorithm (Eq. 1) for the Chesapeake Bay. In spatial distribution, the highest TSS values appear in Upper Bay, western branches, and along the coasts, while lower values are

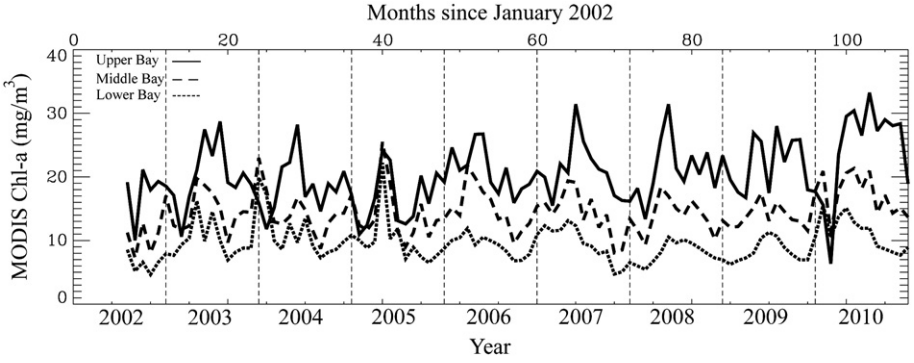

Fig. 8. Time series of mean Chl-a from the MODIS monthly composite images using the NIR-SWIR combined method at the stations for Upper (solid lines), Middle (dashed lines), and Lower (dotted lines) Bays.

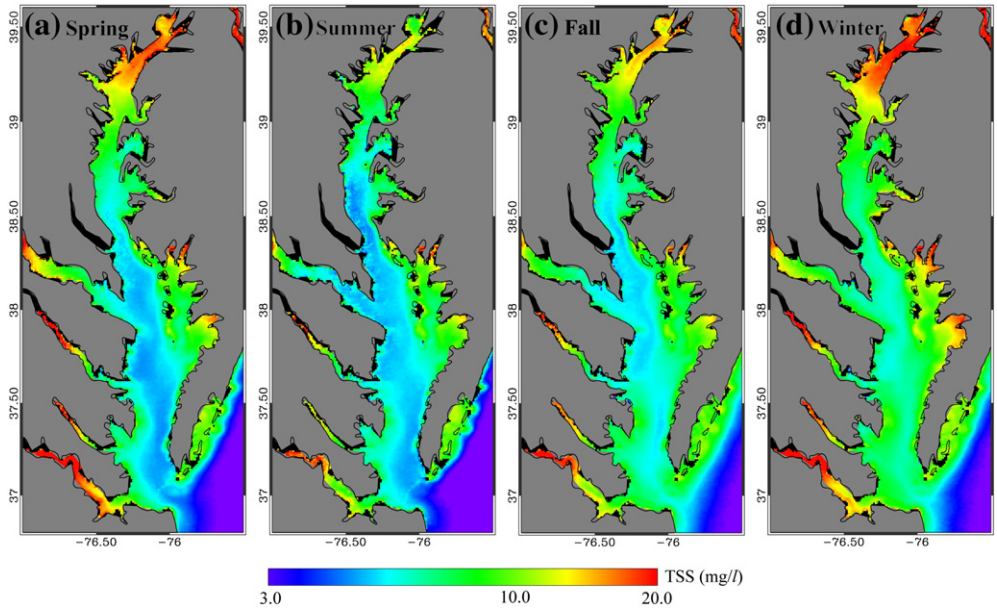

Fig. 9. Seasonal climatology images of the MODIS-Aqua-derived TSS for the period of July 2002 to December 2010 using the NIR-SWIR method in the main stem of the Chesapeake Bay in (a) spring, (b) summer, (c) fall, and (d) winter.

in the central part of the Middle to Lower Bays (particularly in the western section of the main stem region) in all seasons. The highest TSS values appeared in winter (December to February), especially in Upper Bay (Fig. 9d). Relatively high TSS values are in the eastern area of Middle Bay and various branches. In the spring season, the TSS spatial pattern is similar to that in winter, showing high TSS values in Upper Bay and various branches and low values in Middle and Lower Bays. However, some obviously reduced TSS values are observed in spring, particularly in the central part of Middle to Lower Bays (Fig. 9a). The lowest TSS values are in summer over all areas (Fig. 9b). The lowest TSS is geographically located in the western part of Middle Bay and the southeastern part of Lower Bay. The TSS values are slightly increased in the fall season compared with those in summer (Fig. 9c).

Time series of monthly averages of MODIS-Aqua-derived TSS in the Upper, Middle, and Lower Bays from July 2002 to December 2010 are shown in Fig. 10. The seasonal pattern of the MODIS TSS is generally similar in all areas, showing higher values in winter and lower values in late summer to early fall. For the study period, the MODIS-derived TSS values in Middle and Lower Bays are always exceeded by those in the Upper Bay. TSS in Middle Bay is slightly higher than that in Lower Bay. There is, overall, a strong interannual variability in TSS in the Chesapeake Bay. Significantly high TSS values are present in December of 2003 and 2004, as well as in January and April of 2005 in Upper Bay. Relatively lower TSS values appear in fall of 2002 in all areas. Seasonal variability is relatively weak and the magnitudes of TSS values are lower in 2008 and 2009 in Middle and Lower Bays. Overall, the pattern of the TSS time series is more or less similar to that of $nL_w(\lambda)$ from green to NIR bands, in particular, for $nL_w(645)$ as shown in Fig. 6 (Miller & McKee, 2004).

4.6. Satellite climatology images

Fig. 11 provides climatology images (July 2002 to December 2010) of the MODIS-Aqua-derived $nL_w(\lambda)$ at 443, 555, 645, and 859 nm, Chl-a, and TSS using the NIR-SWIR method. Overall, the pattern of MODIS-Aqua-derived $nL_w(\lambda)$ images is similar, showing the highest values in Upper Bay, eastern Mid-South Bay, and the northern area

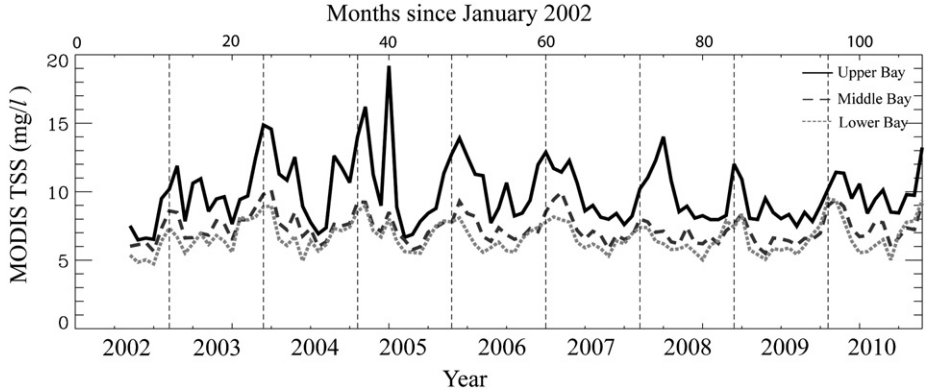

Fig. 10. Time series of mean TSS from the MODIS monthly composite images using the NIR-SWIR combined method at the stations for Upper (solid lines), Middle (dashed lines), and Lower (gray dotted lines) Bays.

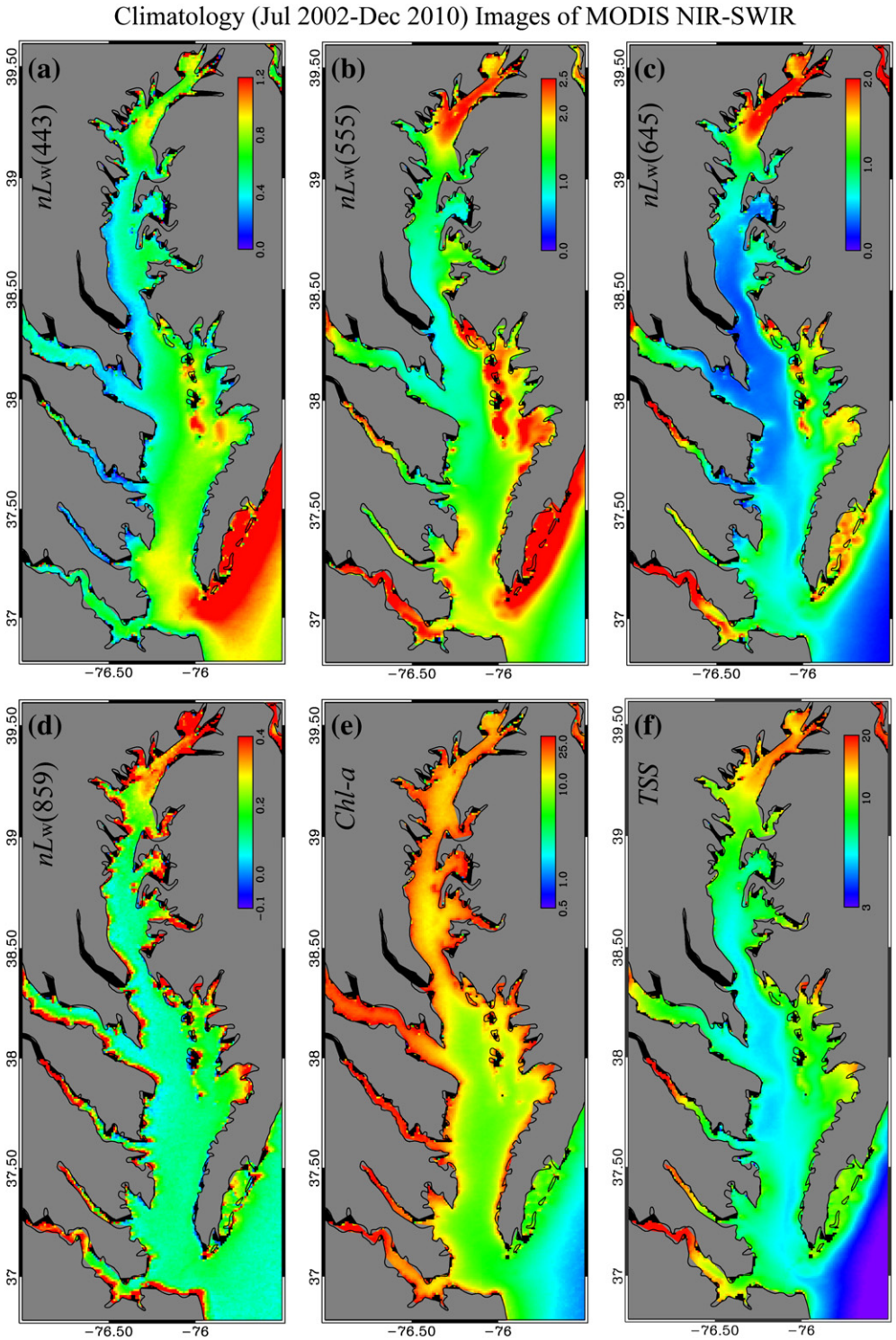

Fig. 11. Climatology composite (July 2002 to December 2010) images of the MODIS-derived (a) $nL_w(443)$, (b) $nL_w(555)$, (c) $nL_w(645)$, (d) $nL_w(859)$, (e) Chl-a, and (f) TSS using the NIR-SWIR method in the Chesapeake Bay. Color scales for $nL_w(443)$, $nL_w(555)$, $nL_w(645)$, and $nL_w(859)$ are 0–1.2, 0–2.5, 0–2.0, and −0.1–0.4 $mW \cdot cm^{-2} \cdot \mu m^{-1} \cdot sr^{-1}$, respectively, while scales (in logarithm) for Chl-a and TSS are 0.5–25 $mg \cdot m^{-3}$ and 3–20 $mg\ l^{-1}$, respectively.

of the Chesapeake Bay's mouth (along the peninsula) and lower values in the western part of Middle Bay. The MODIS $nL_w(443)$ values are relatively higher offshore from the Chesapeake Bay's mouth, compared to the other $nL_w(\lambda)$ images. In addition, significantly high values of the MODIS-Aqua $nL_w(859)$ image appear along the coasts. Generally, distributions of the MODIS-derived Chl-a image are similar to those of the MODIS $nL_w(\lambda)$ images. High Chl-a concentrations appear in Upper Bay, various bay branches, and along the coastal lines, and the lower concentrations are in Lower Bay and outside of the Chesapeake Bay. However, unlike the $nL_w(\lambda)$ images, Chl-a concentrations are relatively high in the western part of Middle Bay. On the other hand, MODIS-derived TSS image shows that significantly high TSS values are in Upper Bay and along the coasts, and the low values are in the central region of Middle to Lower Bays.

5. Discussions and conclusion

Comparison results between MODIS-derived and the in situ-measured $nL_w(\lambda)$ showed that MODIS-Aqua $nL_w(\lambda)$ products using the NIR R2009 method are underestimated in most of the wavelengths. The NIR-SWIR $nL_w(\lambda)$ are improved, but data noise is large most likely due to the lower sensor signal-noise ratio values for the MODIS SWIR bands (Wang & Shi, 2012; Wang et al., 2009b). Our results confirm that the SWIR-based approach provides quantitative improvements in satellite-derived $nL_w(\lambda)$ data in the Chesapeake Bay, where waters are often productive (i.e., there are significant NIR ocean radiance contributions). The $nL_w(\lambda)$ evaluation results in the Chesapeake Bay are consistent with the previous studies (Wang et al., 2009b; Werdell et al., 2009).

For the Chesapeake Bay waters, we used in situ Chl-a measurements from the Water Quality Database to assess the performance of the MODIS-Aqua Chl-a data with the standard-NIR (Ver. 5.2 and R2009) and the combined NIR-SWIR atmospheric correction methods. Results showed that the uncertainty in the MODIS-derived Chl-a data using the NIR-SWIR combined method was reduced compared with that in the MODIS NIR-derived Chl-a data in overall Chesapeake Bay waters. Mean Chl-a values from the NIR Ver. 5.2, NIR R2009, and NIR-SWIR are 19.29, 14.86, and 11.14 $mg \cdot m^{-3}$, respectively, compared with the mean in situ value of 10.28 $mg \cdot m^{-3}$. These correspond to overall Chl-a ratio values (MODIS to in situ) of 1.876, 1.446, and 1.084 from three methods, respectively. The MODIS-derived Chl-a using NIR and NIR-SWIR methods are overestimated in the Middle and Upper Bays of the Chesapeake Bay, in particular, there are significant overestimations in Upper Bay, e.g., in Upper Bay mean Chl-a values from the NIR Ver. 5.2, NIR R2009, and NIR-SWIR are 25.90, 18.83, and 16.03 $mg \cdot m^{-3}$, respectively, compared with the mean in situ value of 12.32 $mg \cdot m^{-3}$. In Lower Bay, the MODIS NIR Chl-a is still overestimated although the MODIS-derived Chl-a data using the NIR R2009 are improved by about 16% compared with those from the previous NIR algorithm (Ver. 5.2). Meanwhile, the NIR-SWIR method provides a considerable improvement in the ocean color satellite-derived Chl-a data in the Chesapeake Bay, e.g., a mean Chl-a ratio of 0.97 (MODIS to in situ) in Lower Bay region. In addition, about 17% more valid pixels appeared in the MODIS ocean color products using the NIR-SWIR method compared with those using the standard-NIR model over the Chesapeake Bay waters. Results show that the existing bio-optical model works properly in the Lower Bay, while for productive and turbid waters in the Middle and Upper Chesapeake Bay regions an appropriate bio-optical model is still an outstanding issue.

A regional TSS algorithm for the ocean color satellite application has been developed using a relationship of the TSS with the diffuse attenuation coefficient at the wavelength of 490 nm $K_d(490)$ for the Chesapeake Bay waters. Since the water properties in the Chesapeake Bay are strongly influenced by suspended sediments mainly from the river discharges and shallow bathymetry, $K_d(490)$ can be a good indicator of the TSS amount in the water. Results show that MODIS-Aqua-derived TSS products using the new regional algorithm are reasonably accurate compared with the in situ TSS measurements in the Chesapeake Bay, with a mean ratio of the TSS (MODIS to in situ) about 1.06.

The MODIS-Aqua images provided the spatial distribution of $nL_w(\lambda)$ at wavelengths of 443, 555, 645, and 859 nm, Chl-a, and TSS in the Chesapeake Bay. The general patterns are similar in most $nL_w(\lambda)$, Chl-a, and TSS images, showing the highest values in Upper Bay, eastern Mid-South Bay, river branches, and along the coastal lines and the lowest values in Lower Bay. However, the MODIS $nL_w(\lambda)$ values are relatively lower in the western part of Middle Bay and higher offshore from the Chesapeake Bay's mouth. The highest values in Upper Bay seem to be influenced by large amounts of TSS concentrations from the river discharges in the Upper Bay region. As described, the MODIS-derived Chl-a products using the NIR-SWIR atmospheric correction method and a standard Chl-a algorithm are still overestimated in Upper Bay, although errors are significantly reduced compared with the results from the standard-NIR atmospheric correction method.

In seasonal patterns, higher values for the $nL_w(\lambda)$ images appear in winter and spring, and relatively lower values are present in summer to fall for most of the Chesapeake Bay regions. The seasonal high $nL_w(\lambda)$ values are due to a large amount of the river discharges and phytoplankton bloom in spring and strong vertical mixing in winter because of high winds. While the seasonal pattern of the MODIS-Aqua-derived TSS images is similar to that of the $nL_w(\lambda)$ images (highs in spring and winter, and lows in summer and fall), the pattern of the MODIS-Aqua-derived Chl-a (phytoplankton) image is different. High Chl-a values are in spring and summer, but relatively low values are in winter. These results are consistent with those from the previous studies (Harding et al., 2002; Malone et al., 1991). In fact, it is characteristic of temperate regions and coastal waters, with the Chesapeake Bay as one of these regions (Longhurst, 2007; Mann & Lazier, 2006).

Time series of monthly averages of the MODIS-Aqua-derived products are constructed for the three regions (Upper, Middle, and Lower Bays) of the Chesapeake Bay to investigate interannual variability. The temporal patterns of the MODIS-derived water property products are generally similar in all locations and years, showing high values in spring and winter and low values in summer and fall for $nL_w(\lambda)$ and TSS, and highs in spring and summer and the lows in fall and winter for Chl-a. However, strong interannual variability appears in all MODIS-derived products over all areas. In addition, $nL_w(\lambda)$ and Chl-a in Lower Bay are out of phase with those in Upper Bay during some years (e.g., winter in 2003–2004 and 2009–2010 for $nL_w(555)$ and Chl-a), while TSS in all Bays is in phase in most of the periods. It has been reported that the strong temporal and spatial variability in phytoplankton biomass and TSS are strongly influenced by seasonal changes in freshwater flows and physical conditions such as tidal currents in the Chesapeake Bay (Harding et al., 2005; Hood et al., 1999). Interannual variations in freshwater flow (mainly from the Susquehanna River located in the northern head of the Chesapeake Bay) strongly influence on the interplay of light and nutrients regulating the phytoplankton growth rate, and are consequently related to interannual variations in phytoplankton abundance in the Chesapeake Bay (Harding, 1994; Harding et al., 2002). However, the response to the freshwater flow would be different depending on the amount and the area. For example, high Chl-a and TSS values in Upper Bay are related to a rapid response to and a larger amount of the freshwater flow from the Susquehanna River (Harding, 1994). The patterns are more or less similar in Middle and Lower Bays and somewhat different in Upper Bay depending on years. The interannual variability of Chl-a is different from that of the $nL_w(\lambda)$ data, while the variability of TSS is more or less similar to $nL_w(\lambda)$ at red band $nL_w(645)$ (as expected).

Acknowledgments

This research was supported by the NASA and NOAA funding and grants; in particular, the project was partly supported by NOAA Ocean Remote Sensing (ORS) funding. We are grateful to the NASA/GSFC Ocean Biology Processing Group for maintaining and distributing the NOMAD data set and the Chesapeake Bay Program for providing the water quality in situ data set. The MODIS L1B data were obtained from the NASA/GSFC MODAPS Service website. We thank two anonymous reviewers for their useful comments. The views, opinions, and findings contained in this paper are those of the authors and should not be construed as an official NOAA or U.S. Government position, policy, or decision.

References

Ahmad, Z., Franz, B. A., McClain, C. R., Kwiatkowska, E. J., Werdell, J., Shettle, E. P., et al. (2010). New aerosol models for the retrieval of aerosol optical thickness and normalized water-leaving radiances from the SeaWiFS and MODIS sensors over coastal regions and open oceans. *Applied Optics*, *49*, 5545–5560.

Bailey, S. W., Franz, B. A., & Werdell, P. J. (2010). Estimation of near-infrared water-leaving reflectance for satellite ocean color data processing. *Optics Express*, *18*, 7521–7527.
Gallegos, C. L., Correll, D., & Pierce, J. W. (1990). Modeling spectral diffuse attenuation, absorption, and scattering coefficients in a turbid estuary. *Limnology and Oceanography*, *35*, 1486–1502.
Gallegos, C. L., & Neale, P. J. (2002). Partitioning spectral absorption in case 2 waters: Discrimination of dissolved and particulate components. *Applied Optics*, *41*, 4220–4232.
Gitelson, A. A., Schalles, J. F., & Hladik, C. M. (2007). Remote chlorophyll-a retrieval in turbid, productive estuaries: Chesapeake Bay case study. *Remote Sensing of Environment*, *109*, 464–472, doi:10.1016/j.rse.2007.01.016.
Gordon, H. R. (1997). Atmospheric correction of ocean color imagery in the earth observing system era. *Journal of Geophysical Research*, *102*, 17081–17106.
Gordon, H. R. (2005). Normalized water-leaving radiance: Revisiting the influence of surface roughness. *Applied Optics*, *44*, 241–248.
Gordon, H. R., & Wang, M. (1994). Retrieval of water-leaving radiance and aerosol optical thickness over the oceans with SeaWiFS: A preliminary algorithm. *Applied Optics*, *33*, 443–452.
Harding, L. W., Jr. (1994). Long-term trends in the distribution of phytoplankton in Chesapeake Bay: Roles of light, nutrients and streamflow. *Marine Ecology Progress Series*, *104*, 267–291.
Harding, L. W., Jr., Magnuson, A., & Mallonee, M. E. (2005). SeaWiFS retrievals of chlorophyll in Chesapeake Bay and the mid-Atlantic bight. *Estuarine, Coastal and Shelf Science*, *62*, 75–94.
Harding, L. W., Jr., Mallonee, M. E., & Perry, E. S. (2002). Toward a predictive understanding of primary productivity in a temperate, partially stratified estuary. *Estuarine, Coastal and Shelf Science*, *55*, 437–463.
Hood, R. R., Wang, H. V., Purcell, J. E., Houde, E. D., & Harding, L. W., Jr. (1999). Modeling particles and pelagic organisms in Chesapeake Bay: Convergent features control plankton distributions. *Journal of Geophysical Research*, *104*, 1223–1243.
IOCCG (2010). Atmospheric correction for remotely-sensed ocean-colour products. In M. Wang (Ed.), *Reports of International Ocean-Color Coordinating Group, No. 10*. Dartmouth, Canada: IOCCG.
Longhurst, A. (2007). *Ecological geography of the sea.* : Elsevier Academic Press Publ. ISBN:978-0-12-45521-1, 560 pp..
Magnuson, A., Harding, L. W., Jr., Mallonee, M. E., & Adolf, J. E. (2004). Bio-optical model for Chesapeake Bay and the Middle Atlantic Bight. *Estuarine, Coastal and Shelf Science*, *61*, 403–424.
Malone, T. C., Ducklow, H. W., Peele, E. R., & Pike, S. E. (1991). Picoplankton carbon flux in Chesapeake Bay. *Marine Ecology Progress Series*, *78*, 11–22.
Mann, K. H., & Lazier, J. R. N. (2006). *Dynamics of marine ecosystems: Biological–physical interactions in the oceans.* Oxford: Blackwell Publishing Ltd. ISBN:1-45051-1118-6.
Miller, R. L., & McKee, B. (2004). Using MODIS Terra 250 m imagery to map concentrations of total suspended matter in coastal waters. *Remote Sensing of Environment*, *93*, 259–266.
Morel, A., & Gentili, G. (1996). Diffuse reflectance of oceanic waters. III. Implication of bidirectionality for the remote-sensing problem. *Applied Optics*, *35*, 4850–4862.
Nezlin, N. P., DiGiacomo, P. M., Diehl, D. W., Jones, B. H., Johnson, S. C., Mengel, M. J., et al. (2008). Stormwater plume detection by MODIS imagery in the southern California coastal ocean. *Estuarine, Coastal and Shelf Science*, *80*, 141–152.
O'Reilly, J. E., Maritorena, S., Mitchell, B. G., Siegel, D. A., Carder, K. L., Garver, S. A., et al. (1998). Ocean color chlorophyll algorithms for SeaWiFS. *Journal of Geophysical Research*, *103*, 24937–24953.
O'Reilly, J. E., Maritorena, S., Siegel, D. A., O'Brien, M. C., Toole, D., Mitchell, B. G., et al. (2000). Ocean color chlorophyll a algorithms for SeaWiFS, OC2 and OC4: Version 4. *SeaWiFS Postlaunch Technical Report Series.* In S. B. Hooker, & E. R. Firestone (Eds.), *NASA Tech. Memo. 2000–206892*. (pp. 8–22) Greenbelt, Maryland: NASA Goddard Space Flight Center.
Ruddick, K. G., Ovidio, F., & Rijkeboer, M. (2000). Atmospheric correction of SeaWiFS imagery for turbid coastal and inland waters. *Applied Optics*, *39*, 897–912.
Schubel, J. P., & Pritchard, D. W. (1986). Responses of upper Chesapeake Bay to variations in discharge of the Susquehanna River. *Estuaries*, *9*, 236–249.
Shi, W., & Wang, M. (2007). Observations of a Hurricane Katrina-induced phytoplankton bloom in the Gulf of Mexico. *Geophysical Research Letters*, *34*, L11607, doi:10.1029/2007GL029724.
Shi, W., & Wang, M. (2008). Three-dimensional observations from MODIS and CALIPSO for ocean responses to cyclone Nargis in the Gulf of Martaban. *Geophysical Research Letters*, *35*, L21603, doi:10.1029/2008GL035279.
Shi, W., & Wang, M. (2009). Green macroalgae blooms in the Yellow Sea during the spring and summer of 2008. *Journal of Geophysical Research*, *114*, C12010, doi:10.1029/2009JC005513.
Shi, W., & Wang, M. (2009). Satellite observations of flood-driven Mississippi River plume in the spring of 2008. *Geophysical Research Letters*, *36*, L07607, doi:10.1029/2009GL037210.
Shi, W., & Wang, M. (2009). An assessment of the black ocean pixel assumption for MODIS SWIR bands. *Remote Sensing of Environment*, *113*, 1587–1597.
Shi, W., & Wang, M. (2010). Satellite observations of the seasonal sediment plume in central East China Sea. *Journal of Marine Systems*, *82*, 280–285, doi:10.1016/j.jmarsys.2010.06.002.
Shi, W., Wang, M., & Jiang, L. (2011). Spring-neap tidal effects on satellite ocean color observations in the Bohai Sea, Yellow Sea, and East China Sea. *Journal of Geophysical Research*, *116*, C12032, doi:10.1029/2010JC007234.
Siegel, D. A., Wang, M., Maritorena, S., & Robinson, W. (2000). Atmospheric correction of satellite ocean color imagery: The black pixel assumption. *Applied Optics*, *39*, 3582–3591.
Son, S., Wang, M., & Shon, J. (2011). Satellite observations of optical and biological properties in the Korean dump site of the Yellow Sea. *Remote Sensing of Environment*, *115*, 562–572, doi:10.1016/j.rse.2010.10.002.
Stumpf, R. P., Arnone, R. A., Gould, R. W., Martinolich, P. M., & Ransibrahmanakul, V. (2003). A partially coupled ocean–atmosphere model for retrieval of water-leaving radiance from SeaWiFS in coastal waters. *SeaWiFS Postlaunch Technical Report Series.* In S. B. Hooker, & E. R. Firestone (Eds.), *NASA Tech. Memo. 2003–206892*, *vol. 22*. (pp. 51–59) Greenbelt, Maryland: NASA Goddard Space Flight Center.
Tzortziou, M., Herman, J. R., Gallegos, C. L., Neale, P. J., Subramanian, A., Harding, L. W., et al. (2006). Bio-optics of the Chesapeake Bay from measurements and radiative transfer closure. *Estuarine, Coastal and Shelf Science*, *68*, 348–362.
Tzortziou, M., Subramanian, A., Herman, J. R., Gallegos, C. L., Neale, P. J., & Harding, L. W. (2007). Remote sensing reflectance and inherent optical properties in the mid Chesapeake Bay. *Estuarine, Coastal and Shelf Science*, *72*, 16–32.
Wang, M. (2006). Effects of ocean surface reflectance variation with solar elevation on normalized water-leaving radiance. *Applied Optics*, *45*, 4122–4128.
Wang, M. (2007). Remote sensing of the ocean contributions from ultraviolet to near-infrared using the shortwave infrared bands: Simulations. *Applied Optics*, *46*, 1535–1547.
Wang, M., & Shi, W. (2005). Estimation of ocean contribution at the MODIS near-infrared wavelengths along the east coast of the U.S.: Two case studies. *Geophysical Research Letters*, *32*, L13606, doi:10.1029/2005GL022917.
Wang, M., & Shi, W. (2007). The NIR-SWIR combined atmospheric correction approach for MODIS ocean color data processing. *Optics Express*, *15*, 15722–15733.
Wang, M., & Shi, W. (2012). Sensor noise effects of the SWIR bands on MODIS-derived ocean color products. *IEEE Transactions on Geoscience and Remote Sensing*, doi:10.1109/TGRS.2012.2183376.
Wang, M., Shi, W., & Tang, J. (2011). Water property monitoring and assessment for China's inland Lake Taihu from MODIS-Aqua measurements. *Remote Sensing of Environment*, *115*, 841–854, doi:10.1016/j.rse.2010.11.012.
Wang, M., Son, S., & Harding, L. W. (2009). Retrieval of diffuse attenuation coefficient in the Chesapeake Bay and turbid ocean regions for satellite ocean color applications. *Journal of Geophysical Research*, *114*, C10011, doi:10.1029/2009JC005286.
Wang, M., Son, S., & Shi, W. (2009). Evaluation of MODIS SWIR and NIR-SWIR atmospheric correction algorithm using SeaBASS data. *Remote Sensing of Environment*, *113*, 635–644.
Wang, M., Tang, J., & Shi, W. (2007). MODIS-derived ocean color products along the China east coastal region. *Geophysical Research Letters*, *34*, L06611, doi:10.1029/2006GL028599.
Werdell, P. J., & Bailey, S. W. (2005). An improved in-situ bio-optical data set for ocean color algorithm development and satellite data product validation. *Remote Sensing of Environment*, *98*, 122–140.
Werdell, P. J., Bailey, S. W., Franz, B. A., Harding, L. W., Jr., Feldman, G. C., & McClain, C. R. (2009). Regional and seasonal variability of chlorophyll-a in Chesapeake Bay as observed by SeaWiFS and MODIS-Aqua. *Remote Sensing of Environment*, *113*, 1319–1330.
Werdell, P. J., Franz, B. A., & Bailey, S. W. (2010). Evaluation of shortwave infrared atmospheric correction for ocean color remote sensing of Chesapeake Bay. *Remote Sensing of Environment*, *114*, 2238–2247, doi:10.1016/j.rse.2010.04.027.
Zawada, D. G., Hu, C., Clayton, T., Chen, Z., Brock, J. C., & Muller-Karger, F. E. (2007). Remote sensing of particle backscattering in Chesapeake Bay: A 6-year SeaWiFS retrospective view. *Estuarine, Coastal and Shelf Science*, *73*, 792–806.